



Evidence of a Third Body and Photometric Solutions of a High Temperature Marginal Contact Binary CW Aqr

A. Vijaya  and K. Sriram

Department of Astronomy, Osmania University 500007, India; astronomyvijaya@gmail.com, astrosriram@yahoo.co.in
Received 2022 November 25; revised 2023 February 1; accepted 2023 February 20; published 2023 April 19

Abstract

Marginal contact binary systems are an important class of binary systems in exploited by astronomers to understand various astrophysical phenomena as they bridge both semi-detached and overcontact stages. We studied the photometric data of CW Aqr using the JCB 1.3 m telescope (JCBT), Kepler, and TESS to understand the period variations and constrain the light curve solutions. We noted that the period of CW Aqr is increasing with a mass transfer rate of $\dot{m} = 7.53 \times 10^{-8} M_{\odot} \text{ yr}^{-1}$ from the secondary to the primary component. We also ascertained cyclic deviations along with a parabolic trend in the $O - C$ diagram. The residuals displayed a sinusoidal trend which was fitted with an LTTE, indicating the presence of a third body with an orbital period of $P_3 \sim 10$ yr and $e = 0.10$. We fitted the JCBT, Kepler, and TESS photometric normalized light curves and noted the mass ratio to be $q \sim 0.32$ for both contact and semi-detached configurations. We identified a temperature difference between the primary and secondary components of ~ 2500 K. No activity signatures were found in the observed light curves which were also evident from the $H\alpha$ line studies where the filled-in effect was not seen. Overall our study suggests that CW Aqr is a marginal contact binary with a low mass ratio evolving toward a semi-detached configuration. However, it may merge if the period increases due to ongoing mass transfer accompanied by a lowering in the mass ratio and later oscillate back to the period-decreasing trend due to angular momentum loss over a few cycles of thermal relaxation oscillations followed by instability.

Key words: (stars:) binaries: eclipsing – Stars – (stars:) binaries (including multiple): close

1. Introduction

Eclipse timing variations play an important role in understanding the period variation in contact binary (CB) systems along with the probable detection of third or tertiary bodies around them (e.g., Hajdu et al. 2019). The detection of a third body not only provides information about the evolution of the system but also helps in understanding the rapidly rotating merger object. The presence of a third body also helps in removing the degeneracy connected to the proposed models such as Kozai cycles with a tidal friction mechanism (e.g., Kiseleva et al. 1998; Naoz & Fabrycky 2014) and core fragmentation processes (Moe & Kratter 2018; Tokovinin 2018). The presence of a third body will help tighten an inner binary and result in very short-period binary systems ($P < 1$ day). The orbital period may change over a few tens of years due to geometric, dynamic, and intrinsic reasons. If the companion is highly convective in nature then the CB will help in losing angular momentum in the form of mass loss or eruption due to magnetic activity (Applegate 1992; Lanza & Rodono 2002). The geometry and dynamics do require a third body which causes quasi-sinusoidal variation along with parabolic variations in the $O - C$ diagram, causing a phenomenon known as the light travel time effect (LITE;

Irwin 1952, 1959). Furthermore, the apsidal motion may also display period changes. Overall the period variations in these systems are due to mass transfer among the binary companions (Lucy 1976; Webbink 2003), which causes increasing and decreasing trends. The mass eruption from the companions also induces a period-increasing trend (Prendergast & Taam 1974).

Based on thermal relaxation oscillation (TRO) theory (Lucy 1976; Lucy & Wilson 1979), marginal CBs are at evolutionary loci around which a CB system oscillates between contact and semi-detached stages. This oscillation occurs over a duration of $\sim 10^7$ yr because of the non-thermal equilibrium. Systems with large temperature differences exhibit a broken contact state with unequal depths in their corresponding light curve (a typical characteristic of β Lyrae type systems) whereas good thermal contact systems display equal depth in the light curve variation (typical W UMa type light curves). These systems exhibit secular periodic variations due to thermal mass transfer between the two components (e.g., van Hamme et al. 2001; Lee & Lee 2006; Zhu et al. 2009). The direction of mass transfer decides the stages, i.e., mass transfer from a more massive component to a less massive component evolves the system from non-contact to a contact state and vice versa. In an excellent review of various types of CBs, Qian et al. (2020) showed that marginal CBs follow a linear relationship between

Table 1
Details about the Variable (V1), Comparison, and Check Stars

Name	α_{J2000}	δ_{J2000}	V	$B-V$	$J-H$
CW Aqr (variable V1)	22 ^h 19 ^m 22 ^s .2	-16°53'33".3	10.64	0.31	0.26
Comparison star	22 ^h 19 ^m 25 ^s .4	-16°52'30".5
Check star	22 ^h 19 ^m 16 ^s .5	-16°52'54".3

the period and radius. This indicates that the respective stellar companions are close to their Roche lobes. Studying the overall structure of such systems provides information on the various astrophysical processes like mass transfer and hence can be useful to predict evolutionary stages.

Hoffmeister (1933) classified CW Aqr as a variable star due to its short orbital period. CW Aqr was first classified as a near contact eclipsing binary (EB) system with a Stroemgren b band magnitude of 10.70 (Malkov et al. 2006). CW Aqr is a bright CB ($V = 10.64$) with $\alpha = 22^{\text{h}}19^{\text{m}}22^{\text{s}}.2$ and $\delta = -16^{\circ}53'33''.3$, and an orbital period of $P = 0.542913$ day. This system is least studied in terms of periodic variation and photometric solutions though it is been observed by the All Sky Automated Survey (ASAS), and the Kepler and TESS observatories. Here we present the photometric studies based on our and satellite observations and we also report spectroscopic observations around the $H\alpha$ line.

2. Observation and Data Analysis

The source CW Aqr was observed from the JCB 1.3 m telescope (JCBT) at Vainu Bappu Observatory (VBO) equipped with a $2\text{k} \times 2\text{k}$ CCD during 2019 September 28–30 and 2019 October 1 with an exposure time of 120 s in the V band (Table 1). We relied on the *apphot* IRAF package to perform the differential photometry. The comparison and check stars are depicted in Figure 1 along with the variable. Generally, these systems exhibit a filled-in effect in $H\alpha$ due to the associated magnetic activity, and hence spectroscopic observation of the variable was performed during the night of 2019 September 10 using the 2.0 m Himalayan Chandra Telescope (HCT) at the Indian Astronomical Observatory (IAO) equipped with the Himalaya Faint Object Spectrograph and Camera (HFOSC) incorporating a $2\text{k} \times 4\text{k}$ CCD and a central region of $2\text{k} \times 2\text{k}$ along with a plate scale of $0''.296 \text{ pixel}^{-1}$ that yields a $10' \times 10'$ field of view. Data were obtained using a combination of a slit (width $1''.92 \times 11'$) and Grism 7, spanning a wavelength range of 3500–7500 Å. This gives a dispersion of $1.5 \text{ \AA pixel}^{-1}$ and a resolution of $\sim 11 \text{ \AA}$. An exposure time of 1800 s with a grating of 167 lines mm^{-1} was applied for both the variable and the spectrophotometric standard (BD+284211). An FeAr arc lamp was used for wavelength calibration. We relied on various tools from IRAF

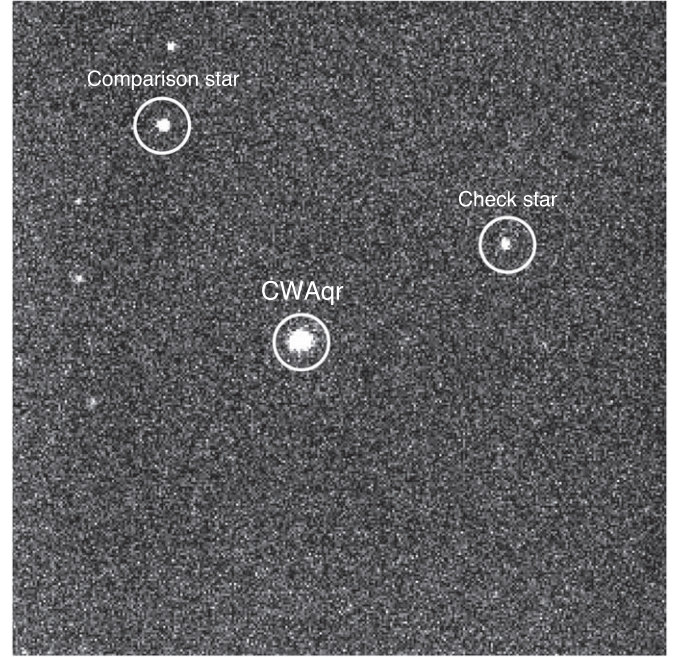


Figure 1. CW Aqr, the comparison star, and the check star are marked in an image taken with the JCBT. The field of view is $7''.46 \times 7''.46$.

to reduce the spectroscopic data. Kepler K2 (EPIC 205934569) and TESS light curves were used to constrain the period variation and derive the photometric solutions.

3. LITE Solutions

The periods were determined for our data, Kepler, TESS, and ASAS data for the CW Aqr using the Period04 program (Lenz & Breger 2005), and times of minima were evaluated. Each time of minimum was checked by inspecting the phased light curves (see Sriram et al. 2018). The ephemeris based on our data was found to be $2,458,757.3134(22) + 0^{\text{d}}.542915(4) E$ (our data), $2,452,520.3590(18) + 0^{\text{d}}.542915(2) E$ (Kepler K2) and $2,452,520.3590(18) + 0^{\text{d}}.542913(3) E$ for TESS data. The ASAS data also revealed a similar period. Overall we used JCBT, Kepler, TESS, and ASAS data to obtain the $O-C$ diagram in order to study the period variation (Table 2). Figure 2 top panel plots the $O-C$ with a dot-dashed line displaying the period-increasing trend.

After fitting the quadratic function we observed a clear cyclic feature that indicates the presence of a third body (Figure 2 top and bottom panels, red line). In order to completely determine the various parameters of the third body assuming cyclic variation, we used Zsche's code (Zsche et al. 2009) in MATLAB which implements the Simplex method in order to arrive at best-fit solutions. The following equation was applied

Table 2

 Observed Times of Minima for CW Aqr from ASAS Database (1), the Kepler K2 Data (2), Tess Data (3), Our Observations (4), $O - C$ Gateway (5), and Bob Nelson's Database (6)

HJD (2450000+)	Error	Epoch	$(O - C)_1$	$(O - C)_2$	Reference
2467.6945	0.0023	-11585	0.02821	-0.00782	1
2467.6959	0.0031	-11585	0.0297	-0.00632	1
2520.3591	0.0025	-11488	0.03014	-0.00546	1
2564.3329	0.0022	-11407	0.2819	-0.00706	1
2736.9809	0.0065	-11089	0.02986	-0.00401	1
2760.8672	0.0062	-11045	0.02869	-0.00499	1
2940.5748	0.0052	-10714	0.03148	-0.00079	1
3166.9685	0.0056	-10297	0.03076	0.00021	1
3562.7529	0.0029	-9568	0.03118	0.00356	1
3973.1938	0.0326	-8812	0.02976	0.00504	6
3980.7923	0.0124	-8798	0.02747	0.00281	6
4291.883	0.0086	-8225	0.02903	0.00648	1
6898.385	0.0216	-3424	0.00571	-0.00224	6
6977.1100	0.0002	-3279	0.00833	0.00073	2
6978.1967	0.0012	-3277	0.00950	0.00190	2
6978.7425	0.0064	-3276	0.00959	0.00200	2
6979.8262	0.0075	-3274	0.00976	0.00217	2
6980.912	0.0006	-3272	0.00994	0.00236	2
6982.5401	0.0215	-3269	0.00920	0.00162	2
6983.6253	0.0068	-3267	0.00937	0.00180	2
6985.2549	0.0046	-3264	0.00963	0.00206	2
6987.4266	0.0007	-3260	0.00998	0.00242	2
6989.0551	0.0062	-3257	0.00924	0.00169	2
6991.2269	0.0051	-3253	0.00959	0.00205	2
6993.9422	0.0006	-3248	0.01002	0.00249	2
6998.8273	0.0049	-3239	0.00881	0.00131	2
7003.1711	0.0094	-3231	0.00950	0.00201	2
7008.5989	0.0007	-3221	0.00837	0.00091	2
7013.4862	0.0068	-3212	0.00916	0.00172	2
7018.3729	0.0058	-3203	0.00994	0.00252	2
7023.2593	0.0005	-3194	0.00972	0.00232	2
7028.1451	0.0054	-3185	0.00951	0.00214	2
7033.0309	0.0097	-3176	0.00929	0.00194	2
7038.4602	0.0064	-3166	0.00916	0.00183	2
7043.3471	0.0025	-3157	0.00994	0.00263	2
7044.9755	0.0215	-3154	0.00920	0.00190	2
7046.0611	0.0021	-3152	0.00938	0.00209	5
8356.1062	0.0091	-739	0.00531	0.00312	5
8741.0169	0.0006	-30	-0.00901	-0.00995	4
8757.3108	0.0075	0	-0.00260	-0.00349	4
8757.3122	0.0152	0	-0.00120	-0.00209	4
8757.3134	0.0076	0	0	-0.00089	4
8787.3147	0.0256	0	0.00130	0.00040	5
8758.9379	0.0064	3	-0.00424	-0.00513	3
9061.8811	0.0125	561	-0.00659	-0.00659	3
9064.5950	0.0006	566	-0.00716	-0.00715	3
9065.1385	0.0068	567	-0.00657	-0.00656	3
9068.3969	0.0054	573	-0.00555	-0.00553	3
9071.1101	0.0215	578	-0.00711	-0.00709	3
9073.8262	0.0257	583	-0.00568	-0.00565	5
9492.9553	0.0652	1355	-0.00521	-0.00408	5

 to the overall $O-C$ diagram (Figure 2, red line)

$$\text{Min.}I = \text{JD}_o + P.E + \frac{Q.E^2}{c} + \frac{a_{12} \sin i}{c} \times \left[\frac{1 - e_3^2}{1 + e_3 \cos \nu} \sin(\nu + \omega_3) + e_3 \sin(\omega_3) \right], \quad (1)$$

where $a_{12} \sin i$, c , e_3 , ν , and ω_3 , are the projected semimajor axis, speed of light, eccentricity, true anomaly of the binary orbit around the center of mass of the triple system, and the longitude of the periastron, respectively. Table 3 displays the best-fit values for various parameters. The eccentricity of the third body was found to be low at $e = 0.10 \pm 0.02$ and the orbital period was found to be about 9.83 ± 0.20 yr (Figure 2, bottom panel). The third body was ascertained to have $0.69 M_\odot$ for $i = 90^\circ$ (see Table 3).

4. Photometric Solutions

Since the source has not been studied hitherto, we performed a detailed photometric solution with our data, and the Kepler and TESS light curves. We used the Physics Of Eclipsing Binaries (PHOEBE) software (Prsa & Zwitter 2005) to perform the photometric analysis which incorporates the Wilson–Devinney methodology (Wilson & Devinney 1971; Wilson 1979, 1990). We applied various techniques to constrain the temperature of the primary component. The color of CW Aqr is $B-V = 0.31$ which corresponds to a temperature of ~ 7200 K (Cox 2000). Poro et al. (2022) studied 204 CBs and reported a regression relation between orbital period and primary component temperature, $T_1 = 6951.42 \times P + 3426.01$. Based on this we found the temperature T_1 of CW Aqr to be 7200 K. We also confirmed the primary temperature based on the relation derived by Sekiguchi & Fukugita (2000) which uses an un-reddened index $(B-V)_o$. We utilized the relation $A_V = R_V \times E(B - V)$ in order to determine $E(B - V)$. We estimated $E(B - V) = 0.03$ for $A_V = 0.093$ (Schlafly & Finkbeiner 2011) which resulted in $(B-V)_o = 7241$ K, in good agreement with other estimated values of the temperature. Hence we adopted the primary component temperature to be $T_1 = 7200$ K. The following methodology was invoked to get the best solution for the light curves (for more details see Sriram et al. 2016, 2017, 2018). We fixed the gravity darkening coefficients $g_1 = g_2 = 0.32$ (Lucy 1967) and adopted albedos $A_1 = A_2 = 0.5$ for both components (Rucinski 1969). Bolometric and bandpass limb darkening coefficients (square root) were referenced from the table published by van Hamme (1993). A circular and synchronous ($F = 1$) orbit was assumed. Initially, four parameters were adjusted, i.e., temperature of the secondary component (T_2), orbital inclination (i), the

5. Discussion and Results

Very few EB systems exhibit the possibility of a third body. Hajdu et al. (2019) found 992 out of 425,193 EBs and there were just 161 systems out of 258 with pure LTTE solutions in the Optical Gravitational Lensing Experiment (OGLE) IV database. The cyclic or quadratic period variation was reported for 126 EAs from a sample of 4683 EAs using Catalina Sky Survey data. Hong et al. (2022) reported 307 CBs with sinusoidal variations and 1–4 CBs with two variations out of 13,716 systems using the OGLE III and IV databases for the Galactic bulge. The third body period was found to be in the range of 5.0–14.0 yr. Scrutinizing OGLE data observed from 1992 to 2000, Kubiak et al. (2006) identified secular period variations in CBs with an orbital period of less than 1 day. Examining a larger sample from OGLE of about 22,462 short-period binaries with periods less than 4 days, Pietrukowicz et al. (2017) found 35 systems with cyclic variations. It is evident that very few systems among EBs exhibit cyclic variation and hence studies in this direction are important as they facilitate the understanding of many astrophysical issues in EBs. In the present work, the residuals clearly exhibit a cyclic trend (top and bottom panels of Figure 2, red line). We found that the orbital period of the third body is around 10 yr with an $e = 0.10$ (see Table 3). This strongly indicates that the third body plays a key role in lowering the angular momentum, resulting in the tightening of the binary (Pribulla & Rucinski 2006). We estimate the mass of the third body to be $0.70 M_{\odot}$ for $i = 90$.

We also found clear evidence of a period-increasing trend in the $O - C$ diagram.

The absolute parameters were obtained using Gazeas's three-dimensional correlations considering both orbital period and mass ratio ($q = 0.32$) parameters, viz. $M_1 = 1.62 M_{\odot}$, $M_2 = 0.52 M_{\odot}$, $R_1 = 1.80 R_{\odot}$, $R_2 = 1.06 R_{\odot}$. The period change was found to be around $1.60 \times 10^{-7} \text{ day yr}^{-1}$ ($0.01384 \text{ s yr}^{-1}$) and the mass transfer rate from the secondary to the primary component was determined using Equation (2) and ascertained to be $7.53 \times 10^{-8} M_{\odot} \text{ yr}^{-1}$.

$$\frac{\dot{P}}{P} = 3\dot{M}_1 \left[\frac{1}{M_1} - \frac{1}{M_2} \right]. \quad (2)$$

The light curve solutions suggest that $q = 0.32$, which is not close to the deep low mass ratio systems ($q = 0.25$), and a secular period increase would further lower the mass ratio due to mass transfer from the secondary to the primary component.

Sometimes the observed cyclic variation could be due to the dynamic effects caused by a third body in these systems (Borkovits et al. 2015). It has a complex dependency on the orbital elements over both the respective orbits, i.e., inner and outer orbits, due to the stellar components and moreover it also affects the relative configuration. This effect will induce an amplitude in the observed $O - C$, similar to LITE. The

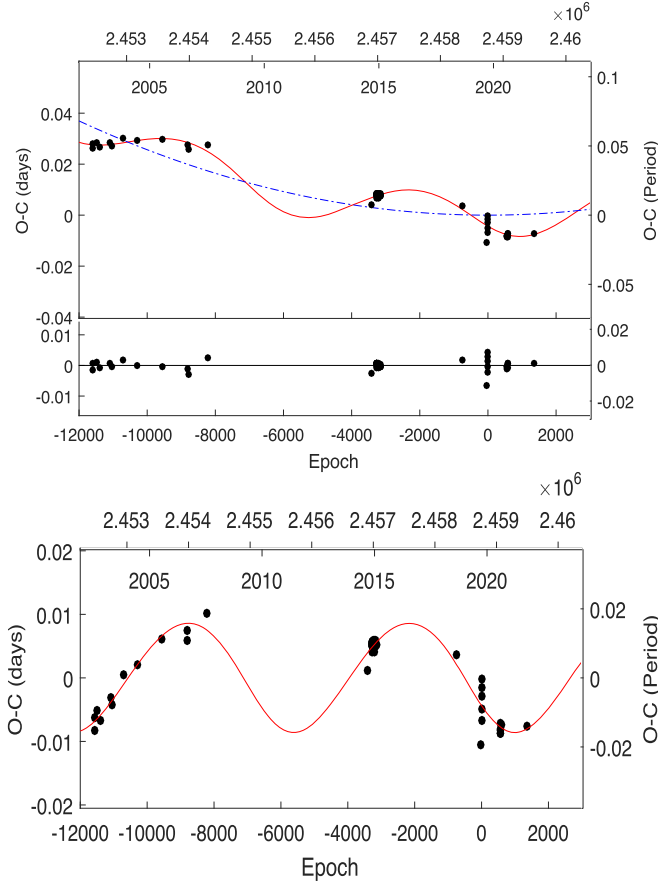


Figure 2. Top panel: $O - C$ diagram obtained from our data ephemeris. The dot-dashed line displays the parabolic fit and the thick line shows the LTTE solution (see Equation (2)) for $e = 0.10$ along with residuals in its lower panel. Bottom panel: zoomed view of the cyclic variation.

dimensionless potentials of the primary and secondary components ($\omega_2 = \omega_1$) (depending on the configuration), and the corresponding bandpass luminosity of the primary star (L_1). We attempted two configurations in order to obtain the solution, i.e., overcontact and semi-detached configurations. Since there is no spectroscopic mass ratio available for this source, we adopted a grid search method to constrain it. The grid search was performed in the range of $0.04 < q < 5$ by varying the adjustable parameters. Later the mass ratio parameters were also freed to get the best fit. The best fit solution resulted in a mass ratio $q = 0.323 \pm 0.006$ and an inclination $i = 72^\circ \pm 0.18$ (Tables 4 and 5, Figures 3 and 4). In order to generate robust the solutions, we varied the inclination by 5% and temperature by 200 K but did not find many variations in the solutions. No O'Connell effect was noticed in the light curve which is also evident for the $H\alpha$ spectral line at different phases (Figure 5). We did not find any filled-in effect which is often considered to be a signature of magnetic activity in these systems (e.g., Sriram et al. 2016).

Table 3
Third-body Solution using LITE (see text for more details)

Parameters	
JD _o (HJD)	2,458,757.3134 ± 0.00075
P, binary period (days)	0.542913 ± 0.000002
Q	1.19144 × 10 ⁻¹⁰ ± 1.13 × 10 ⁻¹¹
A, semi-amplitude (days)	0.00863 ± 0.0006
P ₃ , period (years)	9.83 ± 0.20
e ₃ , eccentricity	0.10 ± 0.02
ω ₃ , longitude of periastron passage	223.10 ± 30.71
T _o , time of periastron passage	2,458,862.254 ± 290.201
a ₁₂ sin i, (AU)	1.492 ± 0.097
f(M ₃), (M _⊙)	0.0343 ± 0.0004
M ₃ (M _⊙) _{i=90°}	0.695 ± 0.003
M ₃ (M _⊙) _{i=60°}	0.824 ± 0.004
M ₃ (M _⊙) _{i=30°}	1.664 ± 0.011

Table 4
Photometric Solutions Obtained for CW Aqr (Overcontact Binary not in Thermal Contact)

Parameter	JCBT	Kepler K2 EPIC	TESS
A ₁ = A ₂	0.50	0.50	0.50
g ₁ = g ₂	0.32	0.32	0.32
T ₁ (K)	7200	7200	7200
T ₂ (K)	4620 ± 69	4568 ± 16	4628 ± 22
q	0.3233 ± 0.0063	0.3295 ± 0.0026	0.3312 ± 0.0036
i°	71.83 ± 0.03	72.03 ± 0.12	74.22 ± 0.35
Ω ₁ = Ω ₂	2.5138 ± 0.0055	2.5262 ± 0.0034	2.5734 ± 0.0084
r ₁ (pole)	0.4502	0.4451	0.4416
r ₁ (side)	0.4829	0.4757	0.4718
r ₁ (back)	0.4991	0.4981	0.4957
r ₂ (pole)	0.2718	0.2504	0.2842
r ₂ (side)	0.2838	0.2593	0.2562
r ₂ (back)	0.2917	0.2844	0.2773
L ₁ /(L ₁ +L ₂)	0.93579	0.97653	0.9225
Σw(O-C) ²	0.0061	0.0052	0.0058

respective amplitudes can be estimated by the following equation (Borkovits et al. 2016)

$$A_{\text{dyn}} = (1/2\pi) * \frac{m_C}{m_{ABC}} \frac{PI^2}{P2} (1 - e_2^2)^{-3/2}, \quad (3)$$

where m_C is the mass of the third component, m_{ABC} is the mass of the total stellar system, PI and $P2$ are the inner and outer periods in units of days respectively, and e_2 is the eccentricity of the third body orbit. We found that A_{dyn} is around 0.00000567 days and the ratio of $A_{\text{dyn}}/A_{\text{LITE}}$ is 0.00065. The low ratio clearly indicates that the observed modulation in $O - C$ is primarily due to the LITE.

Generally when the emission component fills the absorption spectral line features, then it affects the overall shape of the line profile and is considered to be a strong indication of magnetic activity in stellar systems (e.g., Parihar et al. 2009; Sriram et al.

Table 5
Photometric Solutions Obtained for CW Aqr (Primary Star Fills Roche Lobe)

Parameters	JCBT	Kepler K2 EPIC	TESS
A ₁ = A ₂	0.50	0.50	0.50
g ₁ = g ₂	0.32	0.32	0.32
T ₁ (K)	7200	7200	7200
T ₂ (K)	4587 ± 12	4419 ± 91	4494 ± 17
q	0.3213 ± 0.0122	0.3205 ± 0.0032	0.3318 ± 0.0022
i°	71.13 ± 0.15	72.80 ± 0.17	74.78 ± 0.06
Ω ₁	2.3883	2.3903	2.3881
Ω ₂	2.5454 ± 0.0310	2.5553 ± 0.0113	2.5521 ± 0.0044
r ₁ (pole)	0.4302	0.4371	0.4740
r ₁ (side)	0.4556	0.4649	0.4154
r ₁ (back)	0.5716	0.5271	0.5486
r ₁ (point)	0.4966	0.4625	0.4753
r ₂ (pole)	0.2957	0.2427	0.2558
r ₂ (side)	0.3157	0.2514	0.2654
r ₂ (back)	0.2959	0.2773	0.2932
r ₂ (point)	0.3157	0.3026	0.3248
L ₁ /(L ₁ +L ₂)	0.94392	0.970947	0.94013
Σw(O-C) ²	0.0073	0.0053	0.0057

2016, 2017). The H α line is a strong indicator of activity in main sequence (MS) stars (e.g., Boice 1994). We found no filled-in effect in the H α in CW Aqr when observed around secondary and primary eclipses (see Figure 5). During the secondary phase, the secondary stellar component should be along the line of sight pertaining to a low temperature of around ~4600 K (see Tables 4 and 5). Generally at this temperature, the secondary should be associated with strong activity. The absence of activity could be either due to the intrinsic non-active phase of the star or the common convective envelope over the binary hiding the activity. It is predicted that the H α line emission arrives from the upper chromosphere (Houdebine & Doyle 1995). Moreover, the absence of the O'Connell effect in the light curve indicates that during these observations CW Aqr is not associated with any degree of stellar activity. Future spectroscopic observations would be helpful to understand the non-filled-in effect in the spectral lines in CW Aqr.

CW Aqr probably will undergo TRO during which the mass ratio would decrease along with an increase in the orbital period possibly evolving toward a short-period Algol configuration. Later the period may decrease due to mass transfer from the primary to secondary accompanied by angular momentum loss (AML, e.g., Qian 2003) and eventually merge, hence we constrained the possible critical mass ratio. Hut (1980) proposed that binary systems evolve toward instability if the ratio (J_s/J_o) of the total spin of binary components to the total orbital momentum exceeds ~1/3, then instability sets in which triggers the merger. The triggering instability is because the secondary star breaks off the synchronous rotation with

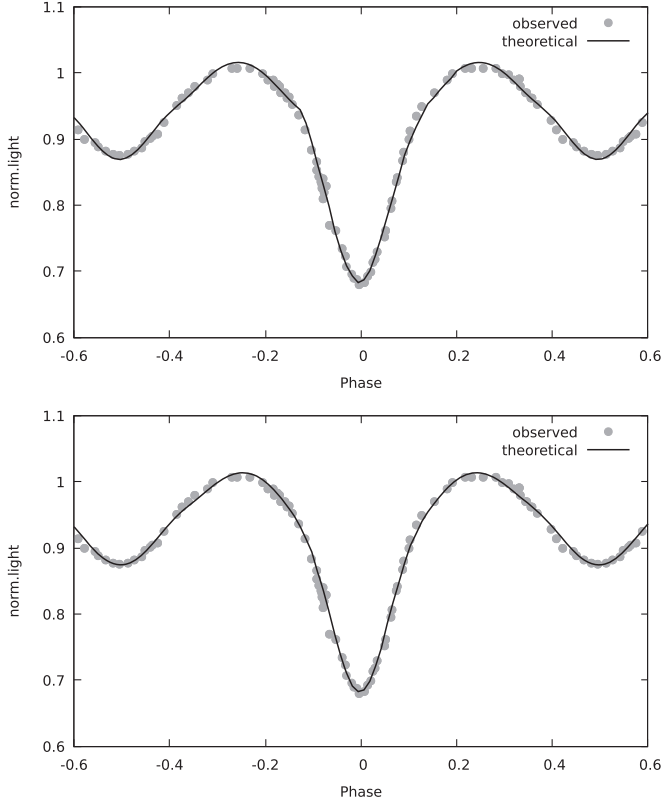


Figure 3. Light curve of CW Aqr (circles) along with their solutions (solid line) when the primary star fills the Roche lobe (top panel) and overcontact binary not in thermal contact configuration (bottom panel).

respect to the primary, due to an increase in the strength of the tidal interaction. To investigate the instability, we calculated the ratio determined by Li & Zhang (2006)

$$\frac{J_s}{J_o} = \left(\frac{1+q}{q} \right) (k_1 r_1)^2 \left(1 + q \left[\frac{k_2}{k_1} \right]^2 \left[\frac{r_2}{r_1} \right]^2 \right), \quad (4)$$

where q is the mass ratio, and k_1 , and k_2 are dimensionless gyration radii of both the components. The exact values of k_1 and k_2 are difficult to calculate as they depend on the structure of each stellar component but an MS star has a value of 0.075 for fully radiative configuration and 0.205 for fully convective configuration. For Sun-like systems $k_1^2 = k_2^2 = k^2 = 0.06$. In CW Aqr, the primary component has a mass of $1.64 M_\odot$ indicating that it has a radiative configuration and the secondary component mass is $0.52 M_\odot$ pertaining to a convective configuration. Assuming $k_1^2 = 0.075$ and $k_2^2 = 0.205$, $J_s/J_o = 1.30$ for $q = 0.32$, which is quite far from the critical momentum ratio of 0.33. For a Sun-like configuration, J_s/J_o is found to be 0.89. We also calculated the ratio using the following relation derived by Landin et al. (2009) which takes into account both tidal and rotational distortion effects on the binary stars. For the primary star mass of $M > 1.4 M_\odot$, $k_1 = 0.175$ considering the relation

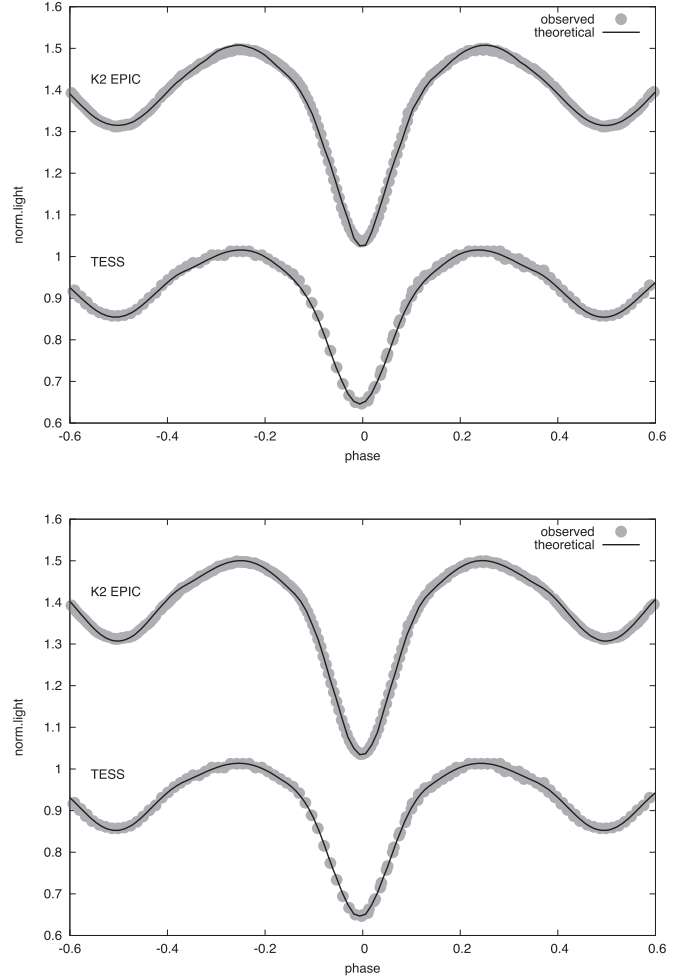


Figure 4. Top (a): K2 EPIC and TESS light curves (circles) along with their solutions (solid lines). (Primary star fills Roche lobe). Bottom panel: K2 EPIC and TESS light curves (circles) along with their solutions (solid lines) (Overcontact binary not in thermal contact). The Kepler K2 light curves are shifted vertically for clarity.

$k_1 = 0.014M + 0.152$. Generally, it has been noted by Jiang et al. (2010) that k^2 increases along with the mass and age of the primary component if its mass $< 1.3 M_\odot$ and the k^2 value saturates above this mass. Using the modified value of k_1 and $k_2^2 = 0.205$, we found the ratio to be $J_s/J_o = 0.71$. This suggests that the system is far from the instability criterion of $J_s/J_o = 0.33$. Wadhwa et al. (2021) estimated an empirical relation to determine the instability mass ratio which is given by $q_{\text{ins}} = 0.0772M_1^2 - 0.3003M_1 + 0.3237$ for fill-out factor $f = 0$ and $q_{\text{ins}} = 0.1269M_1^2 - 0.4496M_1 + 0.4403$ for $f = 1$. We estimated the instability mass ratio to be $q_{\text{ins}} = 0.039$ for $f = 0$ and 0.044 for $f = 1$. This clearly suggests that CW Aqr is far away from the instability mass ratio in order to completely merge further as supported by the estimated period-increasing trend. Based on the estimated mass transfer rate ($7.53 \times 10^{-8} M_\odot \text{ yr}^{-1}$), it will take at least more than $1.38 \times 10^7 \text{ yr}$ ($t = M_2 /$

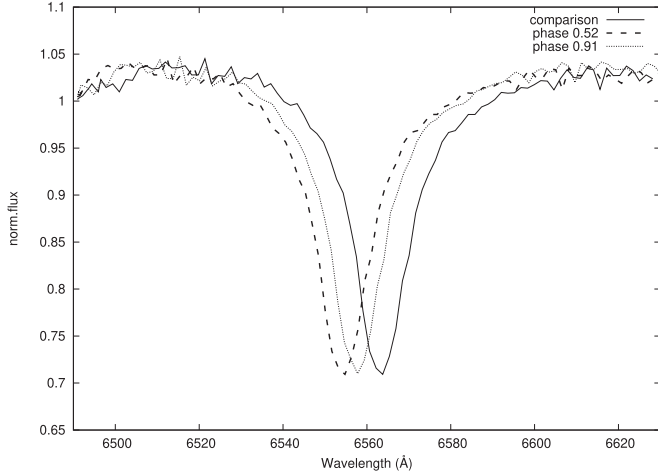


Figure 5. $H\alpha$ spectral line for CW Aqr drawn with a dashed line at two different phases along with the comparisons in terms of normalized flux.

m) to oscillate back until reaching a critical mass ratio and merge.

One can determine the degree of contact stage of a binary *cqby* by determining the orbital angular momentum, J_{orb} (Eker et al. 2006). We determined J_{orb} with the equation $J_{\text{orb}} = 1.24 \times 10^{52} \times M^{5/3} \times P^{1/3} \times q \times (1 + q)^{-2}$ given by Christopoulou & Papageorgiou (2013), where M is the total mass of the binary. We estimated the total mass of the binary applying the relation estimated by Poro et al. (2022) for the primary and using the $q = 0.32$, we determined the secondary mass, and hence the total mass was obtained, i.e., $M = 2.14 M_{\odot}$ and $\log(J_{\text{orb}}) = 51.85$ in cgs units ($\text{g cm}^2 \text{s}^{-1}$). Figure 6 displays the location of CW Aqr with a filled circle symbol along with other marginal CBs in triangle symbols. Other CB data taken from Table 6 exhibit period-increasing trends in their respective $O - C$ which are below the detached system configuration. The data from other systems were taken from Eker et al. (2006). The boundary of the shaded region in Figure 6 is the contact border between the detached (upper portion) and the contact system (shaded region). Based on the photometric solutions, we conclude that CW Aqr is a marginal CB undergoing a secular period increasing trend. The derived potential was $\Omega = 2.5163$ which is close to the inner critical potential ($\Omega_1 = 2.5177$) for our data (see Tables 4 and 5) for the overcontact configuration with a temperature difference), but slightly different from values computed with Kepler and TESS solutions.

Based on $O - C$ variation, CW Aqr's orbital period is found to be secularly increasing at a rate of $\frac{dp}{dt} = 1.60 \times 10^{-7} \text{ day yr}^{-1}$, indicating that mass transfer is occurring from the secondary component to the primary one. The ongoing mass transfer ($\frac{dm}{dt} = 7.53 \times 10^{-8} M_{\odot} \text{ yr}^{-1}$) suggests that material from the secondary is gradually settling down over the primary, resulting in a decrease in the mass ratio of the binary system.

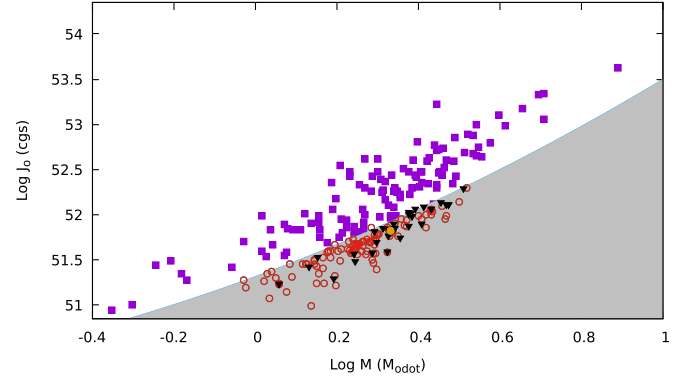


Figure 6. Displaying the location of CW Aqr (orange filled circles) along with a few notable CBs associated with period increasing trend (filled triangles) in the total mass vs. orbital angular momentum diagram. Square boxes are detached binaries and circles correspond to systems with the contact configuration (Eker et al. 2006). The boundary of the shaded region is the border between the detached (upper portion) and contact systems (shaded region).

The loss of mass would occur at a Kelvin–Helmholtz (thermal) timescale $\tau_{\text{KH}} = G M_2^2 / R_2 L_2$ which is estimated to be around $4.28 \times 10^6 \text{ yr}$. From the thermal timescale, the mass transfer rate should be around $M_2 / \tau_{\text{KH}} = 1.21 \times 10^{-7} M_{\odot} \text{ yr}^{-1}$ which is more than that estimated from the $O - C$ diagram. This leads to the conclusion that the transfer of gaseous material from the secondary to the primary is not substantial enough to drive them away from the system to a detached configuration. Table 6 logs the CB parameters with a temperature greater than 6250 K. There is a period increasing ($\frac{dp}{dt} > 0$) trend in the $O - C$ diagram. Based on the data collected, we observed that the mass ratio (q) was found to be varying quadratically with $\frac{dp}{dt}$ (Figure 7). Based on the fits we found the minimum at $q_{\text{min}} = 0.56$, where $\frac{dp}{dt}$ shows the opposite variation. There exists a critical mass ratio of $q = 0.4$ where the CBs are supposed to oscillate and $\frac{dp}{dt}$ changes its trend, i.e., $q < 0.4$ CBs are found to be connected with a period decreasing trend and it increases when $q > 0.4$ (Qian 2003). In our sample all the period-increasing systems peak at the $q = 0.56$ configuration. Around $q = 0.56$, CBs will uniformly tend to move toward relatively higher $\frac{dp}{dt}$. This is possible by mass transfer occurring from the secondary to the primary, eventually forming mostly a low mass ratio system. On the other hand, the high mass ratio systems also tend to evolve toward a lower mass ratio with a similar mass transfer-driven mechanism from secondary to primary. Moreover, it indicates that $q = 0.56$ systems, in general, are biased to evolve toward a lower mass ratio configuration and finally merge as the number of systems is relatively more in the lower mass ratio domain. However, we are limited to discussing further as the number of high mass ratio systems is less (which could be due to non-detection) in general and require further investigations. For a CB to achieve

Table 6
Some Marginal CB Systems with an Increasing Orbital Period

Object Name	$M_1 (M_\odot)$	$M_2 (M_\odot)$	Orbital Period (days)	dp/dt (day yr ⁻¹)	Mass Ratio (q)	T_1 (K)	T_2 (K)	$R_1 (R_\odot)$	$R_2 (R_\odot)$	Reference
CW Aqr	1.62	0.52	0.5429	1.60×10^{-7}	0.320	7200	4620	1.80	1.06	(our source)
TW Crb	1.19	1.28	0.5888	1.50×10^{-7}	0.725	6250	6050	1.44	1.28	(1)
LL Com	1.55	0.43	0.4069	2.62×10^{-7}	0.279	7100	5707	1.34	0.79	(2)
WZ Cyg	1.59	1.00	0.5844	3.78×10^{-8}	0.631	6530	4932	1.72	1.39	(3)
AX Dra	1.46	0.92	0.5681	1.84×10^{-8}	0.743	6850	4947	1.52	1.37	(4)
ZZ Aur	1.62	0.76	0.6012	2.30×10^{-8}	0.511	7800	4978	1.73	1.26	(5)
V836 Cyg	2.20	0.78	0.6534	7.90×10^{-8}	0.357	9790	5462	1.94	1.34	(6)
KW Per	2.78	1.17	0.9312	3.56×10^{-8}	0.420	9340	5213	2.12	1.95	(7)
TT Aur	7.20	4.80	1.3327	1.85×10^{-8}	0.668	23,450	18,000	4.16	4.21	(8)
EG Cep	1.65	0.77	0.5446	3.40×10^{-8}	0.464	7850	5360	1.66	1.18	(9)
CRTS J0121	0.33	1.02	0.3228	6.90×10^{-7}	3.050	5659	5436	0.63	1.04	(10)
V700 Cyg	0.92	0.50	0.2906	0.33×10^{-7}	0.543	5770	6367	0.98	1.26	(11)
AD Cnc	0.90	0.24	0.2827	4.40×10^{-7}	3.744	5164	4609	0.96	0.55	(12)
S Ant	1.94	0.76	0.6483	8.28×10^{-8}	0.392	7800	7340	2.07	1.36	(13), (14)
ϵ Cra	1.76	0.20	0.5914	4.67×10^{-7}	0.114	7100	6639	2.20	0.79	(13), (14)
XZ Leo	1.65	1.20	0.4878	6.02×10^{-8}	0.727	7850	7147	1.50	1.30	(13), (14)
TY Men	1.86	0.40	0.4617	7.23×10^{-7}	0.215	8164	7183	1.85	0.84	(13), (14)
V566 Oph	1.41	0.34	0.4096	2.69×10^{-7}	0.241	6700	6618	1.49	0.76	(13), (14)
TY Pup	2.22	0.72	0.8192	1.66×10^{-7}	0.324	7800	7658	2.73	1.65	(13), (14)
RZ Tau	1.57	0.58	0.4157	9.49×10^{-8}	0.369	7200	7146	1.51	1.00	(13), (14)
DZ Psc	1.37	0.19	0.3661	7.41×10^{-7}	0.136	6210	6195	1.46	0.67	(15)
EF Dra	1.82	0.29	0.4240	5.72×10^{-7}	0.160	6000	6054	1.72	0.80	(16), (14)
UZ Leo	1.69	0.51	0.6180	3.84×10^{-7}	0.303	7250	7780	2.05	2.39	(17), (18), (19)
AG Vir	1.61	0.51	0.6427	4.04×10^{-8}	0.318	7400	700	2.07	1.27	(20)
V535 Ara	2.18	0.79	0.6293	9.36×10^{-7}	0.362	8200	8129	2.03	1.31	(14)
AP Aur	2.05	0.50	0.5693	1.16×10^{-6}	0.247	9016	9328	0.70	1.07	(21), (22)
XY Boo	1.49	0.27	0.3706	6.12×10^{-7}	0.181	7200	7102	0.55	0.25	(23), (13)
RR Cen	1.80	0.32	0.6057	1.98×10^{-7}	0.178	7250	7188	0.55	0.24	(24), (13)
TX Cnc	1.37	0.82	0.3829	5.61×10^{-8}	0.599	6338	6400	0.42	0.33	(25), (13)
DK Cyg	1.82	0.56	0.4706	9.99×10^{-8}	0.307	7500	7011	1.71	1.05	(26)
V401 Cyg	1.68	0.49	0.5827	9.26×10^{-8}	0.300	6700	6650	1.98	1.19	(26), (16)
V728 Her	1.65	0.29	0.4713	3.78×10^{-7}	0.178	6622	6787	1.81	0.92	(14), (16)
UV Lyn	1.34	0.72	0.4150	1.57×10^{-7}	0.530	6709	6290	0.44	0.32	(27), (13)
AV Pup	1.27	1.14	0.4350	4.83×10^{-7}	0.896	6255	6145	1.29	1.23	(28)
V753 Mon	1.59	1.64	0.6770	7.8×10^{-8}	1.031	7728	7669	1.95	1.64	(29)

References: (1) Zhang & Zhang (2003); (2) Ke et al. (2019); (3) Lee et al. (2011); (4) Kim et al. (2004); (5) Oh et al. (2006); (6) Yakut & Eggleton (2005); (7) Galis et al. (2001); (8) Özdemir et al. (2001); (9) Zhu et al. (2009); (10) Shuo et al. (2022); (11) Yang & Dai (2009); (12) Yang & Liu (2002); (13) Maceroni & van't Veer (1996); (14) Qian (2001); (15) Yang et al. (2013); (16) Yakut & Eggleton (2005); (17) Vinkó et al. (1996); (18) Rucinski & Lu (1999); (19) Vinkó et al. (1996); (20) Bell et al. (1990); (21) Agerer & Splittgerber (1993); (22) Li et al. (2001); (23) Molik & Wolf (1998); (24) Bruton & Chambliss (1985); (25) Qian (2001); (26) Wolf et al. (2000); (27) Zhang et al. (1995); (28) Han et al. (2019); (29) Qian et al. (2013).

a low mass ratio, the mass transfer must occur from secondary to primary which further increases the period of the system, and at that stage as the degree of contact lowers, the stellar activity increases which drives the AML. Due to this phenomenon, the period decreases, and the orbit shrinks. Overall CW Aqr will be driven by the TRO mechanism and this oscillation will continue until it encounters instability causing the system to merge. It is observed that the peak is around $q=0.56$, suggesting that the relative energy transfer must accompany the mass transfer rate, and this rate is proportional to the period

change. Such a scenario is observed in the distribution of mass ratio versus relative energy transfer rate which peaks at $q=0.55$ (Li et al. 2008).

Moreover, we noted a temperature difference of ~ 2500 K suggesting that it is at a broken contact stage. The observed potential is close to the value of the inner critical Roche lobe which is a signature of marginal contact systems. In general, these systems have high angular momentum and shallow contact, and sometimes it is difficult to distinguish the source among the phases of the semi-detached or contact stage. These

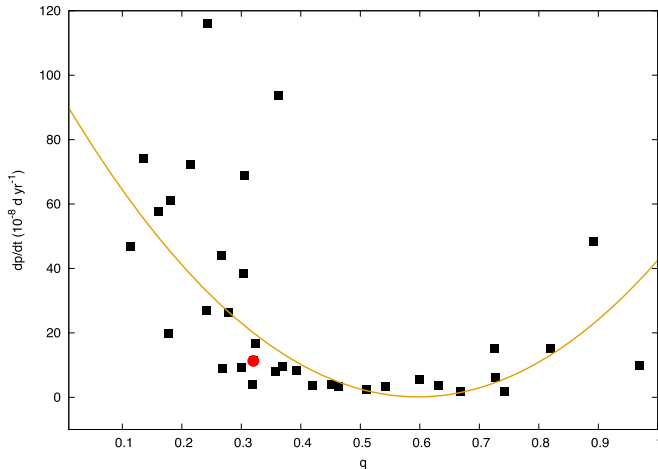


Figure 7. Plot between q (mass ratio) and dp/dt for period increasing CBs in which one of the component temperatures is greater than 6250 K. The line displays the parabolic fit and the filled circle shows the location of CW Aqr. It is clear that most of the systems evolve toward low mass ratio configuration (for more details see text).

systems are interesting as they have arrived at a semi-detached phase from a marginal contact phase via a secular period increase triggered by mass transfer from the secondary to primary. In CW Aqr, we did not notice any signs of magnetic activity, either in the form of the O’Connell effect or the filled-in effect in the $H\alpha$ line, even though the secondary temperature is relatively low. As predicted, these types of systems are going to evolve to a lower degree of contact phase and eventually lower their mass ratio, further decreasing the degree of contact. Later the stellar activity is unveiled, triggering the AML which would tighten the system (e.g., Qian 2001). Moreover, these types of systems are rare as they pass through this near semi-detached phase very quickly. Hence studying such systems is very important. According to the TRO theory (Flannery 1976; Lucy 1976; Robertson & Eggleton 1977), CBs must oscillate between the contact and semi-detached phases. The orbital period should increase in order to reach the semi-detached phase from the shallow contact phase and it must decrease to arrive back to the contact phase. Moreover, the signature of the third body in CW Aqr again demonstrates that it plays a crucial role in removing the angular momentum in order to tighten the binary orbit. Future observations are needed to confirm the solutions, the orbital parameters of the third body and the possible emergence of stellar activity which drives the system to a contact phase configuration.

6. Conclusion

We performed photometric and spectroscopic studies of a marginal CB system CW Aqr which has been not studied extensively. The system exhibits a period-increasing trend at a rate of $0.01384 \text{ s yr}^{-1}$ along with the presence of a third body with a period of $\sim 10 \text{ yr}$ and low eccentricity. The mass ratio

estimated from the photometric solutions to our Kepler K2 and TESS normalized light curves was found to be $q \sim 0.32$ with an inclination of $\sim 72^\circ$. Our study suggests that CW Aqr would essentially merge after a few oscillations between contact and semi-detached phases until it reaches the critical mass ratio driven by the instability, hence future observations are necessary to fully understand the system.

Acknowledgments

We thank the referee for providing suggestions that improved the quality of the paper. K.S. acknowledges the Core Research Grant of SERB, India for the financial support. We acknowledge the Director of IIA, Bangalore for allocating the time for the observations at HCT and VBO. The high-precision continuous photometric data observed by Kepler and TESS were acquired from the Mikulski Archive for Space Telescopes (MAST) and we sincerely acknowledge the teams from the Kepler and TESS projects for their support in supplying this enormous public open resource.

ORCID iDs

A. Vijaya  <https://orcid.org/0000-0003-4852-1756>

References

- Agerer, F., & Splittgerber, E. 1993, *IBVS*, **3942**, 1
- Applegate, J. H. 1992, *AJ*, **385**, 621
- Bell, S. A., Rainger, P. P., & Hilditch, R. W. 1990, *MNRAS*, **247**, 632
- Boice, D. C. 1994, in *ASP Conf. Ser. 64, Coll Stars, Stellar Systems, and the Sun*, ed. J.-P. Caillault (San Francisco, CA: ASP), 684
- Borkovits, T., Rappaport, S., Hajdu, T., & Sztakovics, J. 2015, *MNRAS*, **448**, 946
- Borkovits, T., Hajdu, T., Sztakovics, J., et al. 2016, *MNRAS*, **455**, 4136
- Bruton, J. R., & Chambliss, C. R. 1985, *IBVS*, **3942**, 1
- Christopoulou, & Papageorgiou, A. 2013, *AJ*, **146**, 157
- Cox, A. N. 2000, *Allen’s Astrophysical Quantities* (4th edn.; New York: Springer)
- Eker, Z., Demircan, O., Bilir, S., & Karatas, Y. 2006, *MNRAS*, **373**, 1483
- Flannery, B. P. 1976, *AJ*, **205**, 217
- Galis, R., Hric, L., & Niarchos, P. 2001, *A&A*, **373**, 950
- Hajdu, T., Borkovits, T., Forgács-Dajka, E., et al. 2019, *MNRAS*, **48**, 2562
- Han, Q.-W., Li, L.-F., & Jiang, D.-K. 2019, *RAA*, **19**, 174
- Hoffmeister, C. 1933, *AN*, **247**, 281
- Hong, K., Lee, J. W., Park, J.-H., et al. 2022, *AJ*, **163**, 157
- Houdebine, E. R., & Doyle, J. G. 1995, *A&A*, **302**, 861
- Hut, P. 1980, *A&A*, **92**, 167
- Irwin, J. B. 1952, *AJ*, **116**, 211
- Irwin, J. B. 1959, *AJ*, **64**, 149
- Jiang, D., Han, Z., Wang, J., Jiang, T., & Li, L. 2010, *MNRAS*, **405**, 2485
- Ke, H., Kun, C., Fu-Yuan, X., Yun-Xia, Y., & Er-Gang, Z. 2019, *AJ*, **158**, 104
- Kim, H.-I., Lee, J. W., Kim, C.-H., et al. 2004, *PASP*, **116**, 931
- Kiseleva, L. G., Eggleton, P. P., & Mikkola, S. 1998, *MNRAS*, **300**, 292
- Kubiak, M., Udalski, A., & Szymanski, M. K. 2006, *AcA*, **56**, 253
- Landin, N. R., Mendes, L. T. S., & Vaz, L. P. R. 2009, *A&A*, **494**, 209
- Lanza, A. F., & Rodono, M. 2002, *AN*, **323**, 424
- Lee, C.-U., & Lee, J. W. 2006, *J. Korean Astron. Soc.*, **39**, 25
- Lee, J. W., Kim, S. L., Lee, C. U., et al. 2011, *AJ*, **142**, 12
- Lenz, P., & Breger, M. 2005, *CoAst*, **144**, 41
- Li, L., Liu, Q., Zhang, F., & Han, Z. 2001, *AJ*, **121**, 1091
- Li, L., & Zhang, F. 2006, *MNRAS*, **369**, 2001
- Li, L., Zhang, F., Han, Z., Jiang, D., & Jiang, T. 2008, *MNRAS*, **387**, 97

- Lucy, L. B. 1976, [ApJ](#), **205**, 208
- Lucy, L. B., & Wilson, R. E. 1979, [ApJ](#), **231**, 502
- Maceroni, C., & van't Veer, F. 1996, [A&A](#), **311**, 523
- Malkov, O. Yu., Oblak, E., Snegireva, E. A., & Torra, J. 2006, [A&A](#), **446**, 785
- Moe, M., & Kratter, K. M. 2018, [ApJ](#), **854**, 44
- Molík, P., & Wolf, M. 1998, [IBVS](#), **4640**, 1
- Naoz, S., & Fabrycky, D. C. 2014, [ApJ](#), **793**, 137
- Oh, K. D., Kim, C.-H., Lee, W.-B., Kim, H.-i., & Kang, Y. W. 2006, [MNRAS](#), **366**, 1243
- Özdemir, S., Ak, H., Tanriver, M., et al. 2001, [PASA](#), **18**, 151
- Parihar, P., Messina, S., Bama, P., et al. 2009, [MNRAS](#), **395**, 593
- Pietrukowicz, P., Soszynski, I., Udalski, A., et al. 2017, [AcA](#), **67**, 115
- Porro, A., Sarabi, S., Zamanpour, S., et al. 2022, [MNRAS](#), **510**, 5315
- Prendergast, K., & Taam, R. 1974, [ApJ](#), **189**, 125
- Pribulla, T., & Rucinski, S. M. 2006, [AJ](#), **131**, 2986
- Prsa, A., & Zwitter, T. 2005, [ApJ](#), **628**, 426
- Qian, S. B. 2001, [MNRAS](#), **328**, 914
- Qian, S. B. 2003, [MNRAS](#), **342**, 1260
- Qian, S. B., Zhang, J., Wang, J. J., et al. 2013, [ApJS](#), **207**, 22
- Qian, S. B., Zhu, L.-Y., Liu, L., et al. 2020, [RAA](#), **20**, 163
- Robertson, J. A., & Eggleton, P. P. 1977, [MNRAS](#), **179**, 359
- Rucinski, S. M., & Lu, W. X. 1999, [AJ](#), **118**, 2451
- Schlafly, E. F., & Finkbeiner, D. P. 2011, [ApJ](#), **737**, 103
- Sekiguchi, M., & Fukugita, M. 2000, [AJ](#), **120**, 1072
- Shuo, M., Jin-Zhong, L., Yu, Z., Qingshun, H., & Guo-Liang, L. 2022, [RAA](#), **22**, 095017
- Sriram, K., Malu, S., Choi, C. S., & Vivekananda Rao, P. 2016, [AJ](#), **151**, 69
- Sriram, K., Malu, S., Choi, C. S., & Vivekananda Rao, P. 2017, [AJ](#), **153**, 231
- Sriram, K., Malu, S., Choi, C. S., & Vivekananda Rao, P. 2018, [AJ](#), **155**, 172
- Tokovinin, A. 2018, [AJ](#), **155**, 160
- van Hamme, W. 1993, [AJ](#), **106**, 2096
- van Hamme, W., Samec, R. G., Gothard, N. W., et al. 2001, [AJ](#), **122**, 3436
- Vinkó, J., Hegedüs, T., & Hendry, P. D. 1996, [MNRAS](#), **280**, 489
- Wadhwa, S. S., De Horta, A. Y., Filipovic, M. D., et al. 2021, [MNRAS](#), **501**, 229
- Webbink, R. F. 2003, in ASP Conf. Ser. 293, 3D Stellar Evolution, ed. S. C. Turcotte & R. M. Keller (San Francisco, CA: ASP), 76
- Wilson, R. E. 1979, [ApJ](#), **234**, 1054
- Wilson, R. E. 1990, [ApJ](#), **356**, 613
- Wilson, R. E., & Devinney, E. J. 1971, [ApJ](#), **166**, 605
- Wolf, M., Molík, P., Hornoch, K., et al. 2000, [A&AS](#), **147**, 243
- Yakut, K., & Eggleton, P. P. 2005, [AJ](#), **629**, 1055
- Yang, Y. G., & Dai, H. F. 2009, [PASJ](#), **61**, 577
- Yang, Y.-G., Qian, S. B., Zhang, L. Y., Dai, H. F., & Soonthornthum, B. 2013, [AJ](#), **146**, 35
- Yang, Y.-L., & Liu, Q.-Y. 2002, [CJAA](#), **4**, 369
- Zasche, P., Liakos, A., Niarchos, P., et al. 2009, [NewA](#), **14**, 121
- Zhang, X. B., & Zhang, R. X. 2003, [AJ](#), **125**, 1431
- Zhang, X. B., Zhang, R. X., Zhai, D. S., & Fang, M. J. 1995, [IBVS](#), **4240**, 1
- Zhu, L.-Y., Qian, S.-B., Liao, W. P., et al. 2009, [PASJ](#), **61**, 529
- Zhu, L. Y., Qian, S. B., Zola, S., & Kreiner, J. M. 2009, [AJ](#), **137**, 3574